



# Experimental Study of the Mechanical Characteristics of Jinping Marble Under Multi-stage True Triaxial Compression Testing

Gang Wang<sup>1</sup> · Xia-Ting Feng<sup>1</sup> · Chengxiang Yang<sup>1</sup> · Qiang Han<sup>1</sup> · Rui Kong<sup>1</sup>

Received: 8 January 2021 / Accepted: 2 November 2021 / Published online: 13 November 2021  
© The Author(s), under exclusive licence to Springer-Verlag GmbH Austria, part of Springer Nature 2021

## Abstract

Because true triaxial compression testing is generally more complicated, time-consuming, and expensive than conventional triaxial compression testing, further research is needed to reduce the cost and time of true triaxial compression tests. In this study, the true triaxial apparatus developed by Northeastern University is used, which can change the principal stress in one direction independently. Multi-stage true triaxial compression tests are carried out on Jinping marble, and the effectiveness of the new test method is evaluated. The strength parameters obtained from the multi-stage tests and single-stage tests are compared. It is suggested that constant slope unloading should be carried out before the peak strength to ensure reliable and effective experimental results. The multi-stage true triaxial compression test exhibits good repeatability and can obtain reliable strength parameters in a short time for reference in engineering practice. Under different multi-stage loading conditions, Jinping marble presents different strength, deformation and failure characteristics, and the macrofailure mechanical properties of a specimen are affected by the propagation of microcracks within that specimen.

**Keywords** Multi-stage true triaxial compression test · Jinping marble · Strength · Deformation characteristics

## Abbreviations

$\sigma_1, \sigma_2, \text{ and } \sigma_3$	Maximum, intermediate, and minimum principal stresses, respectively
$\varepsilon_1, \varepsilon_2, \text{ and } \varepsilon_3$	Maximum, intermediate, and minimum principal strains, respectively
$\varepsilon_v$	Volumetric strain
$\tau_{\text{oct}}$	Octahedral shear stress
$\sigma_{m,2}$	Mean effective normal stress
$a, b$	Material constants
$d\sigma$	Absolute increment of $\sigma_1$ in each stage of unloading
$E_1$	Deformation modulus
$\sigma_{cd}$	Crack damage stress
$\mu_{21}^e \text{ and } \mu_{31}^e$	Strain increment ratios in the intermediate and minimum principal stress directions, respectively

## 1 Introduction

Laboratory tests are usually required to obtain the parameters for engineering design and numerical calculation (Martin 1997; Feng 2017). The parameters of rocks under high stresses can be obtained from true triaxial compression testing (Mogi 1977; Chang and Haimon 2000; Feng et al. 2016). However, current true triaxial testing also presents some challenges. Normally, the number of standard specimens used in true triaxial compression tests under the same  $\sigma_2$  condition should not be less than three (Zhang et al. 2019a, b). Sometimes, because of complicated geological conditions, the dispersion of the processed specimens is large, so the deviation in the strength results is large. In this case, it is possible that the parameters obtained by regression analysis also have large errors. In addition, sometimes, the number of cores obtained from on-site drilling or on-site rock blocks is limited, which may affect the acquisition of test results, because laboratory tests require many standard specimens. Considerable time and costs are required to perform the true triaxial compression tests and obtain a complete set of results, which may affect the progress of the project. Therefore, it is necessary to further study practical test methods to reduce the dispersion problem and reduce the cost and time of laboratory rock mechanics tests.

✉ Xia-Ting Feng  
fengxiating@mail.neu.edu.cn

<sup>1</sup> Key Laboratory of Ministry of Education on Safe Mining of Deep Metal Mines, Northeastern University, Shenyang, China

The true triaxial multi-stage loading test is a promising test. At present, the conventional triaxial multi-stage loading test has been widely used (Dassanayake et al. 2015; Bondarenko et al. 2017; Tsoi and Homenok 2017; Wild et al. 2017). The conventional triaxial multi-stage loading test was first proposed by Taylor (1951) to measure the shear strength of silty sand, but Taylor pointed out that the multi-stage test is applicable to only specimens that are not sensitive to structural changes. Kim and Ko (1979) proposed that the multi-stage loading test can reduce the discreteness of a specimen. By comparing the test results of the single-stage and multi-stage tests, the feasibility of multi-stage loading is validated. The International Society for Rock Mechanics (ISRM) proposed and validated a multi-stage triaxial testing method (Kovari et al. 1983), which was also validated by Pagoulatos (2004). Li et al. (2005) conducted multi-stage triaxial compression tests on two types of UK coal measure rocks at different saturation levels and found that jointed rocks respond more strongly to water than intact rocks. Youn and Tonon (2010) proposed a radial strain control method suitable for triaxial multi-stage loading tests on brittle rocks and suggested the use of a partial stress–radial strain curve to determine the imminent failure point. Yang (2012) conducted a multi-stage triaxial loading test on red sandstone, analyzed its strength and deformation behavior, proposed a strength correction method, and proved its rationality. In summary, scholars have conducted a large number of studies on the conventional triaxial multi-stage loading tests and obtained reliable test results. However, no research has been published on the comprehensive and critical assessment of the suitability of true triaxial multi-stage loading tests.

The main purpose of this study was to investigate the effectiveness of performing a true triaxial multi-stage loading test on marble from the China Jinping underground laboratory (CJPL-II). A multi-stage loading test was performed on Jinping marble under three conditions, and the influence of different test conditions on the test results was analyzed. The multi-stage loading test data are compared with the true triaxial single-stage loading test data, and the reliability of the test results is studied. Based on this research, a suggestion for carrying out a true triaxial multi-stage loading test is proposed to ensure the reliability of Jinping marble multi-stage loading data. The effects of microcracks on the strength, deformation, and failure modes of Jinping marble during multi-stage loading were analyzed.

## 2 Experimental Method

### 2.1 Specimen Preparation

The rock specimens were from the deep tunnels of CJPL-II in China. The specimens were collected from gray marble

with a fine-grained crystal structure and no obvious joints. To reduce the test error caused by the individual differences between the specimens, the specimens were taken from the same block of marble, and the rock specimens were processed into  $50 \times 50 \times 100 \text{ mm}^3$  rectangular standard specimens according to the method recommended by ISRM (Feng et al. 2019a). Wave velocity and density tests were performed under natural air-drying conditions, and specimens with abnormal wave velocity and density were excluded. The rock specimens contained two main mineral components, namely, dolomite (89.1%) and calcite (10.9%), and the density was approximately  $2.82 \text{ g/cm}^3$ . The P wave velocity of the rock samples was approximately  $4170.0 \text{ m/s}$  (Xu et al. 2019).

### 2.2 Equipment and Experimental Procedure

True triaxial multi-stage loading experiments were conducted using Northeastern University's true triaxial apparatus (TTA), which has been described in detail by Feng et al. (2016). The  $\sigma_1$  and  $\sigma_2$  actuator output forces of the TTA were 3000 and 6000 kN, respectively, and the maximum design capacity of the confining pressure was 100 MPa. It can apply three-dimensional principal stresses to rock specimens independently and uniformly along the three principal stress directions and can accurately measure the principal strains in the three corresponding principal directions.

In the case of difficult sampling and specimen preparation conditions, multi-stage loading tests have been widely used. Unlike a conventional true triaxial compression test using multiple specimens, true triaxial multi-stage loading experiments use a single rock specimen and compress the sample in stages. The stress path is shown in Fig. 1. In addition to unloading near the peak strength, the multi-stage loading test in this study follows the ISRM recommended method (Feng et al. 2019a). The relationship between the force in the direction of  $\sigma_1$  (LC01, kN) and the corresponding displacement (LVDT05, mm) is continuously monitored during the test. When the slope of the LC01 and LVDT05 curves reaches 100–200 kN/mm (the point at this time is defined as the unloading point, and the strength value of this point is defined as the unloading point strength), the  $\sigma_1$  is unloaded at the rate of 2500 N/s. For the increasing  $\sigma_2$  multi-stage loading test, the  $\sigma_1$  is unloaded to the  $\sigma_2$  level (Fig. 1a), and for the increasing  $\sigma_3$  and conventional triaxial multi-stage loading tests, the  $\sigma_1$  is unloaded to the  $\sigma_3$  level (Fig. 1b and c). Figure 2 shows a typical test result of an increasing  $\sigma_2$  true triaxial multi-stage loading test. At the end of this stage, further loading is carried out according to the test scheme, and the first stage of the test is repeated to observe the influence of multi-stage loading on the specimen.

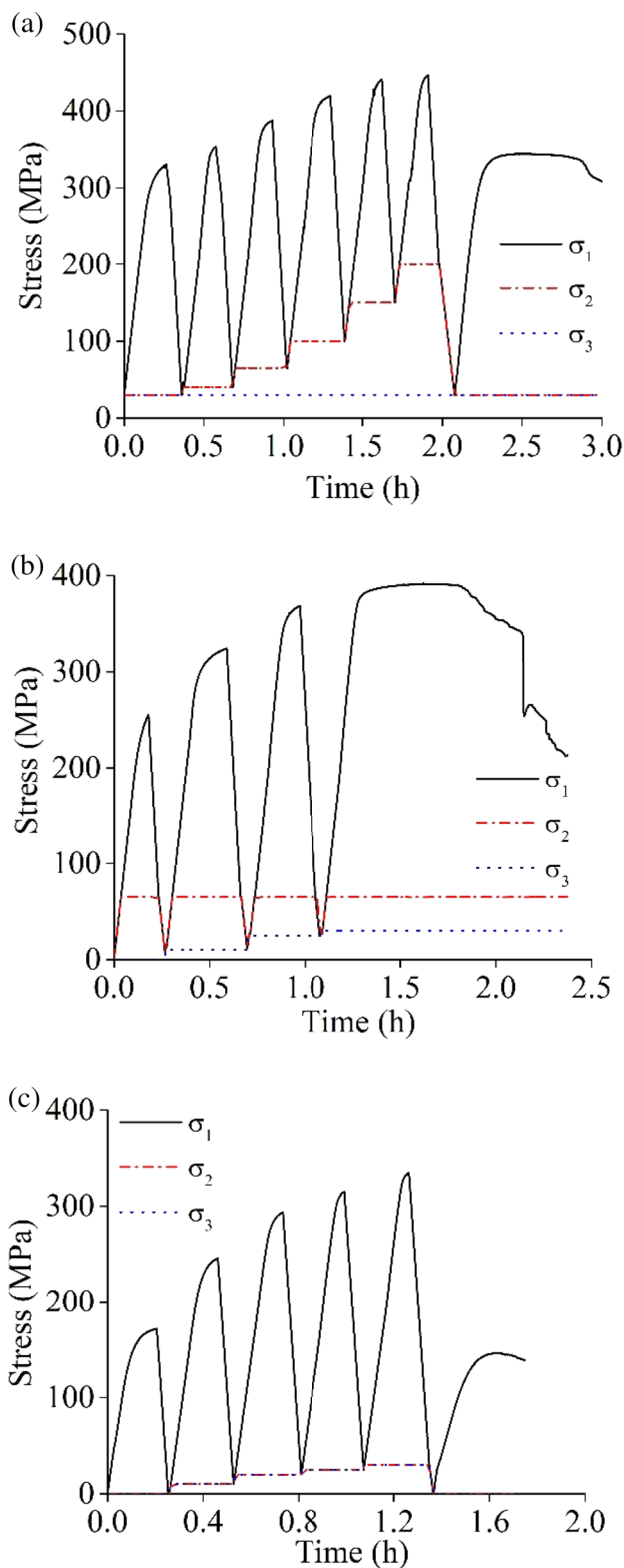


**Fig. 1** Stress path of true triaxial multi-stage loading test. **a** Increasing  $\sigma_2$ . **b** Increasing  $\sigma_3$ . **c** Increasing  $\sigma_2$  and  $\sigma_3$

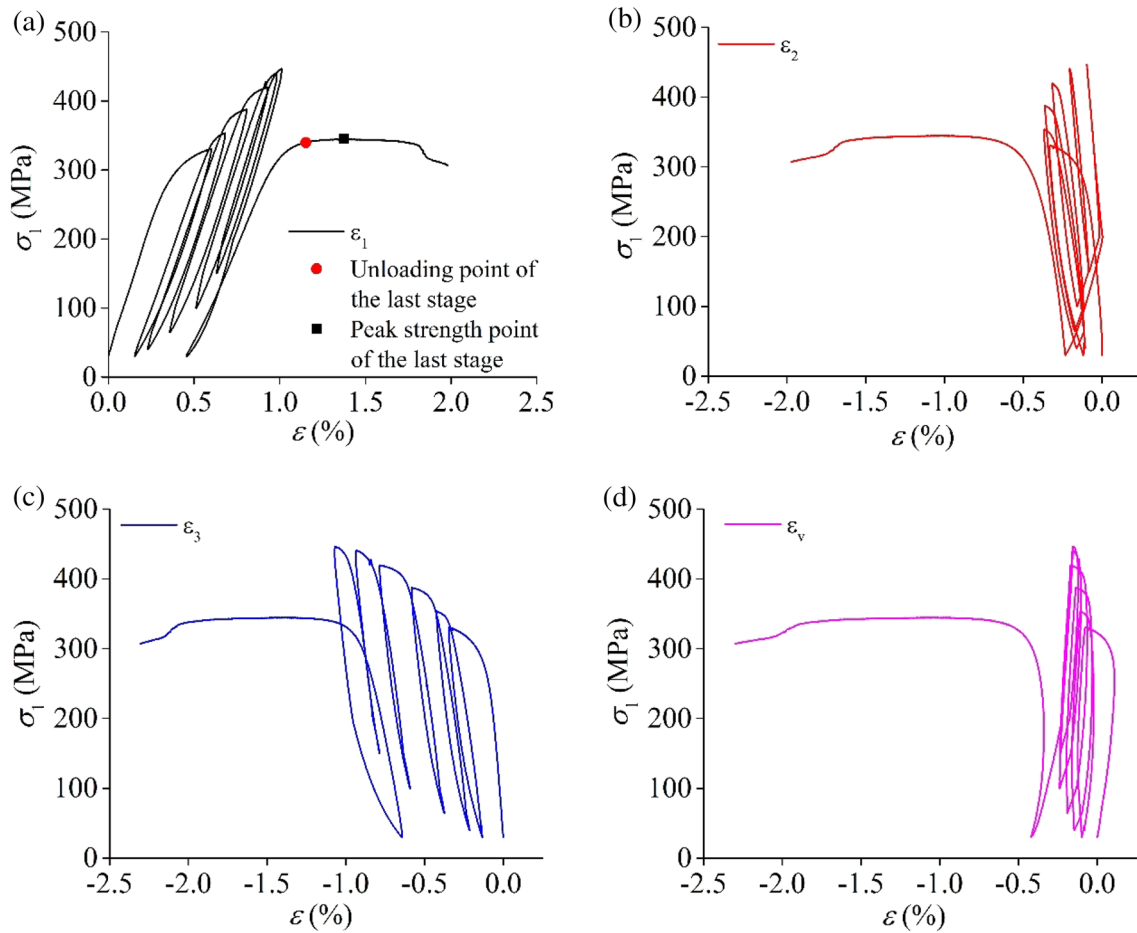
### 3 Validation of the True Triaxial Multi-stage Loading Test

In this study, the results of the multi-stage loading tests are validated. The specific validation is carried out as follows.

#### 3.1 Selection of the Unloading Point

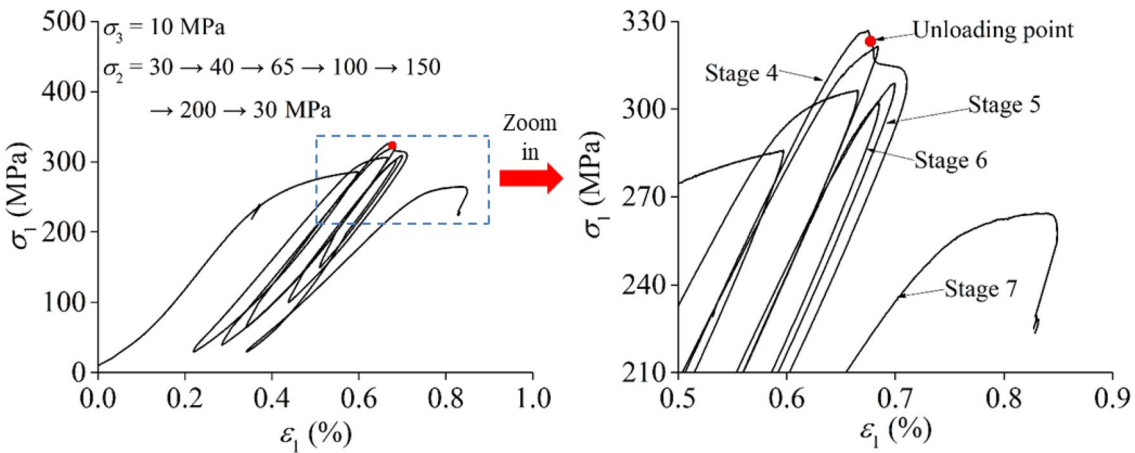
There are many studies on the conventional triaxial multi-stage loading test, but few on the true triaxial multi-stage loading test. The selection of the unloading point of the multi-stage loading test is of great concern, and the accuracy of the test results is greatly affected by the selection of the unloading point. The selection of the unloading point near the peak value of the true triaxial multi-stage loading test can refer to the design of the conventional triaxial multi-stage loading test. There are two methods to select the unloading point according to the stress–strain curve in the conventional triaxial multi-stage loading test: (1) the point where the slope of the stress vs. displacement curve approaches zero (prepeak) (Kovari et al. 1983) and (2) the point at which the deviatoric stress drops from the peak stress to a certain value (postpeak) (Yang 2012). However, the first method only indicates that when the slope of the stress–displacement curve is close to 0, the peak stress point of this stage corresponds to the strength of the rock specimen, and the specific slope is not defined. Thus, it is not easy to unify the unloading points of each stage. After the rock specimen reaches the peak strength, macrocracks begin to appear, and the stress drop caused by the local crack convergence easily appears in the strain softening stage. The existence of macrocracks considerably affects the strength of the next stage, so the second method also has limitations. In summary, it is suggested that the peak strength should not be exceeded for each stage of the true triaxial multi-stage loading test and that unloading should be carried out before the peak strength is reached rather than after the peak strength is reached. Before the test, a large number of marble true triaxial compression test results were statistically analyzed (Xu et al. 2019; Feng et al. 2020, 2021). When the slope of the force–displacement curve is between 100 and 200 kN/mm, the strength is very close to the peak strength.

Figure 3 shows a typical postpeak unloading test result, in which only the unloading point of the fourth stage is marked. In the fourth stage of the test,  $\sigma_2$  is 150 MPa, and unloading occurs after the peak strength is reached. Crack growth and penetration occur after the peak, and then, the  $\sigma_2$  is increased to 200 MPa. According to the test results obtained by Feng et al. (2019b), the peak stress should increase, but the curve shows that although the  $\sigma_2$  is increased, the peak stress is reduced. The test results in Fig. 2 exhibit unloading before



**Fig. 2** Typical test results of increasing  $\sigma_2$  true triaxial multi-stage loading test ( $\sigma_3=30$  MPa;  $\sigma_2=30 \rightarrow 40 \rightarrow 65 \rightarrow 100 \rightarrow 150 \rightarrow 200 \rightarrow 30$  MPa). **a** Stress-strain relationship in  $\sigma_1$  direction. **b** Stress-strain

relationship in  $\sigma_2$  direction. **c** Stress-strain relationship in  $\sigma_3$  direction. **d** Relationship between  $\sigma_1$  and  $\epsilon_v$



**Fig. 3** Examples of unsuited true triaxial multi-stage loading test results

the peak strength, and the strength of the first stage is basically the same as the strength of the last stage. In Fig. 3, the fourth stage of unloading occurs after the peak, and the strength of the last stage is significantly lower than the

strength of the first stage. It can be concluded from the above findings that it is best to ensure that the unloading strength does not exceed the peak strength to avoid the influence of macrocracks on the test results.

To determine the close degree between the unloading point strength and the real peak strength of the specimen, the last stage of the test is continuously loaded to the residual stage. In the last stage, the unloading point can be found by measuring the slope (the unloading step is not carried out), so the unloading strength and peak strength of the specimen can be obtained and compared conveniently. Figure 2a shows a typical result of an increasing  $\sigma_2$  multi-stage loading test, and Fig. 4 shows a typical result of an increasing  $\sigma_3$  multi-stage loading test. The red dot in these figures is the strength of the unloading point in the last stage, and the black square dot is the true peak strength in the last stage. The unloading point strength and the true peak strength in the last stage of the increased  $\sigma_2$  multi-stage loading test are 339 MPa and 345 MPa, respectively, and the unloading point strength and the true peak strength in the last stage of the increased  $\sigma_3$  multi-stage loading test are 382 MPa and 392 MPa, respectively. The difference between the unloading point strength and the real peak value in the last stage is very small. In the last stage, the unloading point strength was only 1.8–3% lower than the true peak strength. Figures 2a and 4 also illustrate the importance of the final stage of loading in the multi-stage loading test, i.e., the validity of determining the unloading point by the slope of the curve before the peak can be validated.

### 3.2 Repeatability Test

Another effective method used to verify the validity of the true triaxial multi-stage loading test is the repeatability test. As shown in Fig. 5a, three specimens of Jinping marble are tested in five stages. The prepeak deformation results of the three tests are basically the same; however, there is little deviation

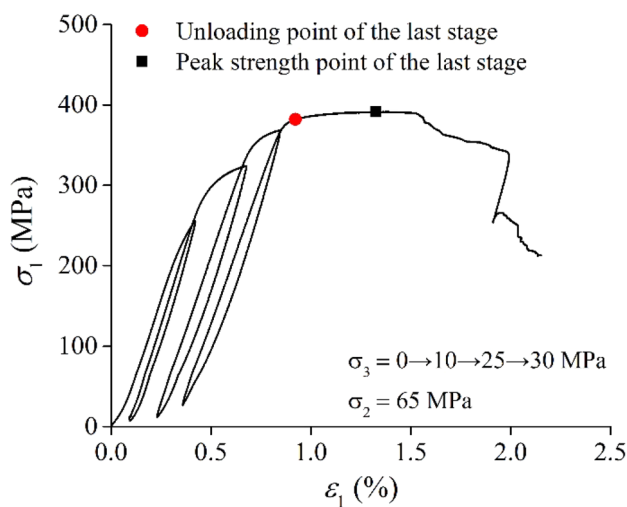


Fig. 4 Determining the proximity of the unloading point strength to the true peak strength of the specimen

after the peak strength due to the uncertainty in postpeak rock specimen fracturing, but the repeatability of the three curves is generally good. Figure 5b shows that the strength results obtained by the three tests are almost the same. The Mogi–Coulomb criterion (Al-Ajmi and Zimmerman 2005) is used to fit the strength of the three tests. The results are shown in Fig. 5c. The three fitting lines almost coincide. The calculated parameters are shown in Table 1. A comparison of the parameters of the three specimens shows that the values of  $b$  and  $\varphi$  are exactly the same for these specimens, and the values of  $a$  and  $c$  are also very close. Therefore, the true triaxial multi-stage loading test also produces good repeatability, which indicates that the multi-stage loading test can provide test results with low discreteness.

### 3.3 Strength Comparison Between Multi-stage Loading and Single-Stage Loading Conditions

To verify the reliability of the true triaxial multi-stage loading test results, the results of the multi-stage loading test are compared with the results of the single-stage loading test. Figure 6a indicates that although the peak strength from the multi-stage loading test is slightly lower than that of the single-stage loading test, the trend of peak strength changing with the  $\sigma_2$  is consistent. The Mogi–Coulomb strength criterion (Al-Ajmi and Zimmerman 2005, 2006) is used to fit the two test results, and the fitting results are shown in Fig. 6b. According to the parameter values obtained from the fitting curve equation, the  $c$  and  $\varphi$  values of the rock specimens in Table 2 under two different loading paths can be obtained. The results in Table 2 show that under the two kinds of loading paths, the values of  $c$ ,  $\varphi$ ,  $a$ , and  $b$  obtained by fitting are similar, which proves the reliability of the strength results obtained in multi-stage loading tests.

## 4 Mechanical Characteristics of Jinping Marble During True Triaxial Multi-stage Loading Testing

In this study, the unloading section of each stage is selected to calculate the deformation modulus  $E_1$  and strain increment ratio of a specimen. Figure 7 shows the method for determining the elastic parameters in the third stage of a test, in which  $d\sigma_1$  is determined from the unloading point strength to the determined  $\sigma_2$  strength level. The defined strain increment ratios have physical meanings and are easy to understand. The specific calculation formulas are as follows:

$$E_1 = \frac{d\sigma_1}{d\varepsilon_1^e} \tag{1}$$

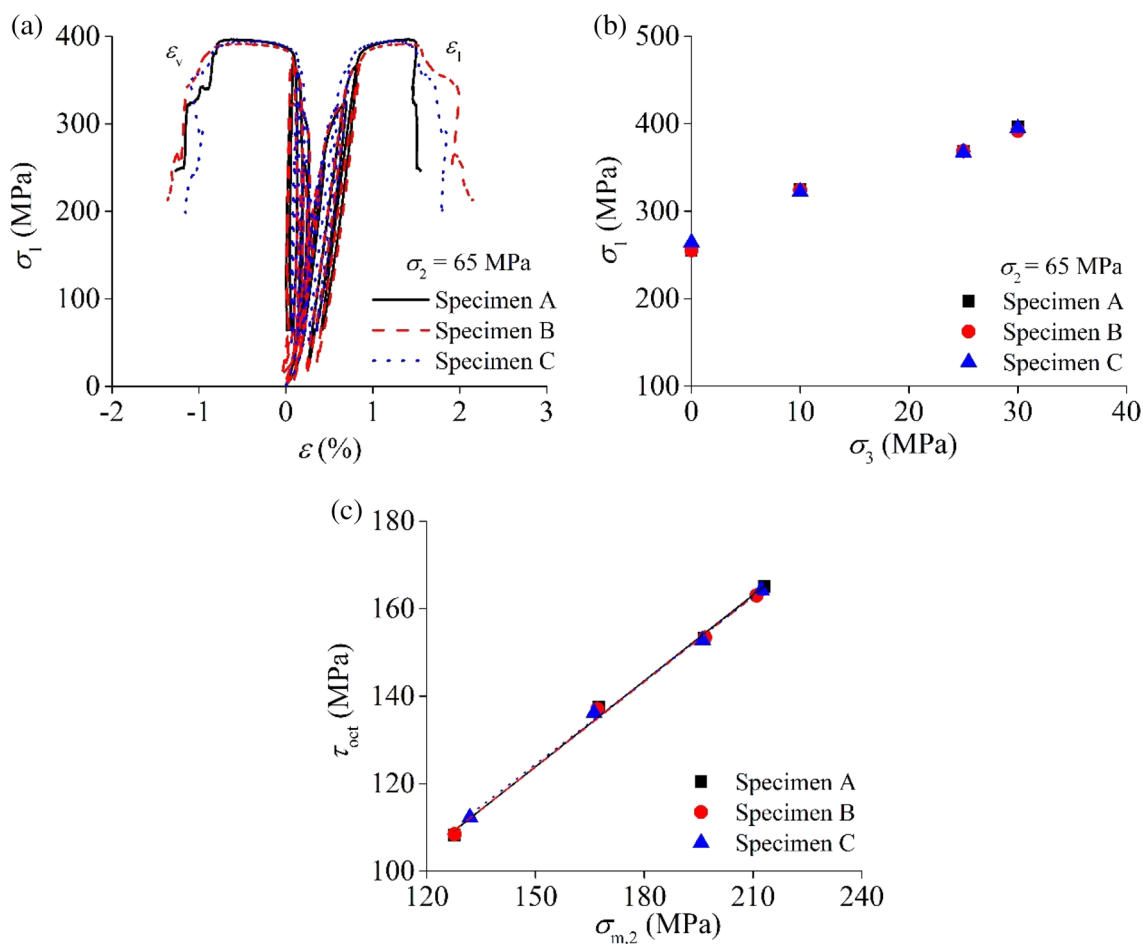


**Fig. 5** Test results obtained from the repeatability tests on marble specimens. **a** Comparison of stress–strain curves. **b** Strength comparison. **c** Mogi–Coulomb strength data fitting for the repeatability test

**Table 1** Mogi–Coulomb strength criteria fitting results and values of  $c$ ,  $\varphi$  of three multi-stage true triaxial tests

Test type	$a$ (MPa)	$b$	$R^2$	$c$ (MPa)	$\varphi$ (°)
Test 1	26.54	0.65	0.99	38.86	43.58
Test 2	25.74	0.65	0.99	37.7	43.58
Test 3	28.8	0.64	0.99	41	42.75

$$\mu_{21}^e = -\frac{d\epsilon_2^e}{d\epsilon_1^e} \tag{2}$$

$$\mu_{31}^e = -\frac{d\epsilon_3^e}{d\epsilon_1^e}, \tag{3}$$

where  $E_1$  is the deformation modulus in the  $\sigma_1$  direction,  $\mu_{21}^e$  and  $\mu_{31}^e$  are the elastic strain increment ratios in the  $\sigma_2$  and

$\sigma_3$  directions, respectively;  $d\sigma_1$  is the absolute increment of  $\sigma_1$  in each stage of unloading; and  $d\epsilon_1^e$ ,  $d\epsilon_2^e$ , and  $d\epsilon_3^e$  are the elastic strain increments in the principal stress directions in each stage, respectively.

### 4.1 Evolution of the Deformation Modulus in the Multi-stage Loading Test

Figure 8 shows the change in deformation modulus with the stress level in three true triaxial multi-stage loading tests. Figure 8a shows the results of the multi-stage loading test with increasing  $\sigma_2$ . The figure shows that the deformation modulus of the specimen basically increases linearly with increasing  $\sigma_2$ . During the process of compaction and release, some defects are not completely released during unloading. In multi-stage loading test of increasing  $\sigma_2$ , as the initiation and propagation of microcracks tend to parallel to the  $\sigma_2$  direction, the rock changes from the weak part and the hard part bearing the internal stress together to the hard part bearing the internal stress alone, or the hard part mainly

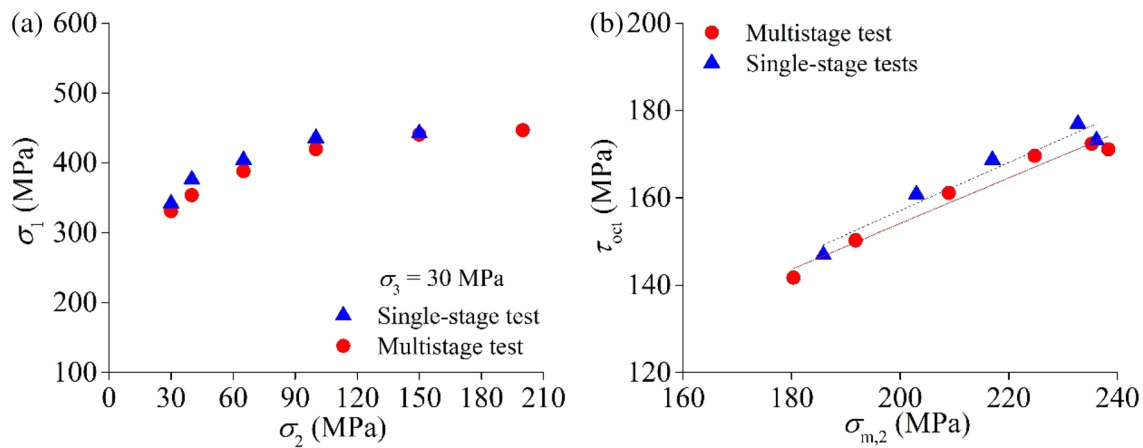


**Fig. 6** Comparison between single-stage tests and multi-stage test. **a** Strength comparison. **b** Mogi-Coulomb strength data fitting comparison

**Table 2** Mogi–Coulomb strength criteria fitting results and values of  $c$ ,  $\varphi$  of Jinping marble specimens under single-stage true triaxial tests and multi-stage true triaxial tests ( $\sigma_3 = 30$  MPa)

Test type	$a$ (MPa)	$b$	$R^2$	$c$ (MPa)	$\varphi$ (°)
Single stage loading test	46.73	0.55	0.92	61.02	35.69
Multi-stage loading test	49.75	0.52	0.96	63.26	33.47

bearing the internal stress, and the rock deformation modulus is strengthened.

Figure 8b shows the results of two multi-stage loading tests with increasing  $\sigma_3$ . The deformation modulus decreases with increasing  $\sigma_3$ , because the increase in  $\sigma_3$  limits the initiation and propagation of microcracks parallel to the  $\sigma_2$  direction. Although microcracks parallel to the  $\sigma_2$  direction initiated in the previous loading stage, with an increase in  $\sigma_3$ , the microcracks became compacted, and the microcracks along the original weak part will be produced in the other directions, resulting in a decrease in the deformation modulus. Increasing  $\sigma_2$  will promote the initiation and propagation of microcracks parallel to the  $\sigma_2$  direction, and increasing  $\sigma_3$  will inhibit the initiation and propagation of microcracks parallel to the  $\sigma_2$  direction, resulting in different  $E_1$  trends in the two tests.

Figure 8c shows the results of the conventional triaxial multi-stage loading test. After confining pressure is applied, the deformation modulus  $E$  of the specimen increases, but the increase amplitude decreases gradually. The reason for this observation is that the increase in confining pressure causes the microfractures inside marble to compact, resulting in an increase in the deformation modulus in the second stage. When loading and unloading continue, the microcracks in the rock will propagate in each cycle of loading and unloading, leading to the gradual accumulation of rock damage. However, due to the compaction induced by the

confining pressure, the intensity and speed of the accumulated damage in the rock are very low, so the deformation modulus shows a basically unchanged trend.

### 4.2 Evolution of $\sigma_{cd}$ in the Multi-stage Loading Test

Figure 9 shows the changes in  $\sigma_{cd}$  with the stress level determined from three true triaxial multi-stage loading tests. Figure 9a indicates that  $\sigma_{cd}$  in the first stage of the multi-stage loading test with increasing  $\sigma_2$  is larger than that in the second stage,  $\sigma_{cd}$  in the last stage is lower than that in the first stage, and  $\sigma_{cd}$  in the middle stage basically increases linearly with increasing  $\sigma_2$ . Figure 9b shows the results of the two multi-stage loading tests with increasing  $\sigma_3$ . Although  $\sigma_{cd}$  fluctuated with increasing  $\sigma_3$ , it basically showed an increasing trend. Figure 9c shows that  $\sigma_{cd}$  basically increases linearly under the conventional triaxial multi-stage loading with increasing confining pressure, and the  $\sigma_{cd}$  of the last stage is far less than that of the first stage. Thus, irreversible loss is produced in the specimen after multi-stage loading, which can be validated from Fig. 1c; that is, the specimen strength in the last stage of conventional triaxial multi-stage loading is less than that in the first stage.

### 4.3 Evolution of the Strain Increment Ratio in the Multi-stage Loading Test

Figure 10 shows the change in the strain increment ratio with the stress level in the  $\sigma_2$  direction. Figure 10a shows that the  $\mu_{21}^e$  obtained in the multi-stage loading test with increasing  $\sigma_2$  decreases. With the increase in the  $\sigma_2$ , the microfractures mainly develop parallel to the  $\sigma_2$  direction (Kong et al. 2018), so  $\mu_{21}^e$  is mainly controlled by the  $\sigma_2$ . The deformation ability of the specimen in the  $\sigma_2$  direction is restrained, resulting in a smaller strain increment ratio. Figure 10b shows the results of the multi-stage

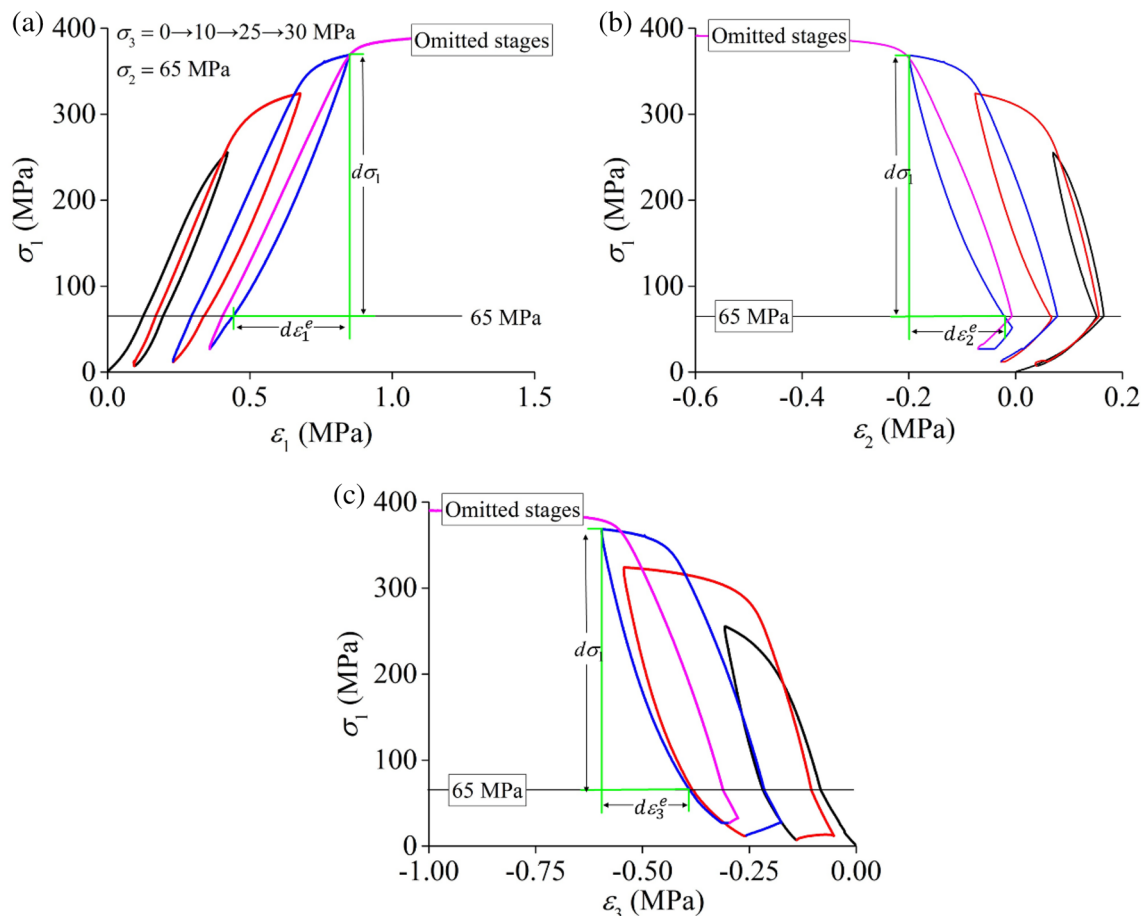


**Fig. 7** Schematic diagram of the methods used to determine the elastic parameters in the true triaxial multi-stage test: **a**  $\sigma_1$  direction, **b**  $\sigma_2$  direction, and **c**  $\sigma_3$  direction

loading test with increasing  $\sigma_3$ ;  $\mu_{21}^e$  increases with increasing  $\sigma_3$ , because with the increase in  $\sigma_3$ , the test conditions approach those of a conventional triaxial test. The microfractures develop from the direction parallel to  $\sigma_2$  toward all directions, resulting in an increase in the deformation of the specimen in the  $\sigma_2$  direction and thus an increase in  $\mu_{21}^e$ . Figure 10c shows that for the results of conventional triaxial multi-stage loading,  $\mu_{21}^e$  increases first and then slightly decreases with increasing confining pressure. This is because after the first stage of loading, microcracks develop in different directions within the specimen, resulting in the deformation capacity of the specimen in the  $\sigma_2$  direction being greater than that in the  $\sigma_1$  direction, so  $\mu_{21}^e$  increases accordingly. After unloading, the adjustment of microcracks in the rock is basically completed, even though some microcracks are not completely released. When the multi-stage loading and unloading process continues, the microcracks in the rock will cause new fracture growth in each cycle of loading and unloading, resulting in the gradual accumulation of rock damage. However, due to the compaction effect of confining pressure, the

deformation capacity of the specimen in the  $\sigma_2$  direction is restrained, resulting in a slight decrease in  $\mu_{21}^e$ .

Figure 11 shows the variation in  $\mu_{31}^e$  for different multi-stage loading tests. Figure 11a indicates that the  $\mu_{31}^e$  obtained in the multi-stage loading test with increasing  $\sigma_2$  decreases. According to the previous analysis, the deformation modulus increases with the increase in  $\sigma_2$ , indicating that the  $\sigma_2$  has a hardening effect on the specimen. The relationship between the strain increment ratio and the deformation modulus indicates that the strain increment ratio of the specimen should decrease; however, due to the influence of the  $\sigma_2$ , the decrease in  $\mu_{21}^e$  is greater, and the rate of decrease in  $\mu_{31}^e$  is relatively low. As shown in Fig. 11b, the damage effect of the rock caused by microcrack fracture propagation in the rock is smaller than the compaction effect of the confining pressure, resulting in the increase in the deformation of the specimen in the  $\sigma_2$  direction and thus the increase in  $\mu_{31}^e$ . With increasing confining pressure, the  $\mu_{31}^e$  of the conventional triaxial multi-stage loading test shows the same trend as  $\mu_{21}^e$  (Fig. 11c), and its mechanical mechanism is also the same.



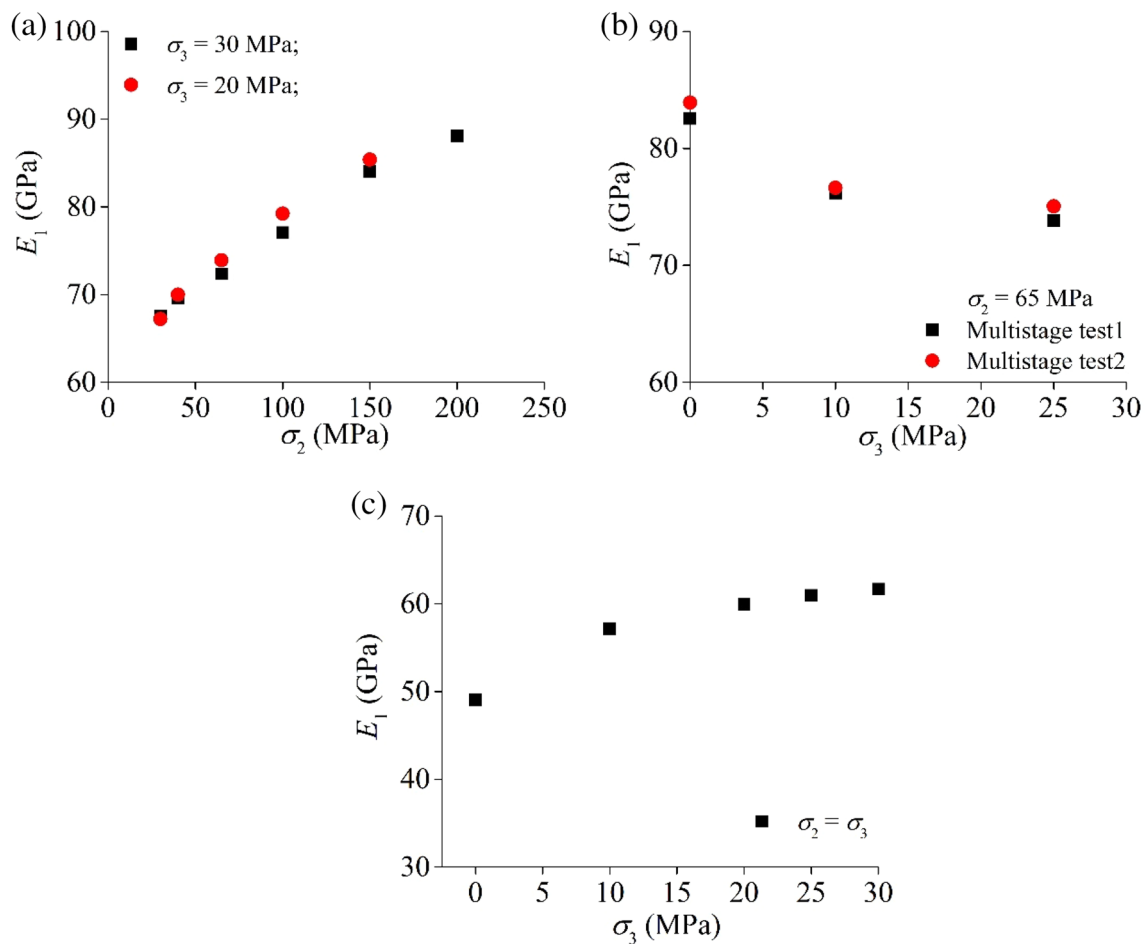


**Fig. 8** Deformation modulus of Jinping marble from the true triaxial multi-stage loading tests. **a** Increasing  $\sigma_2$ . **b** Increasing  $\sigma_3$ . **c** Increasing  $\sigma_2$  and  $\sigma_3$

### 4.4 Failure Mode

The failure mode of the specimen is an important feature of its failure mechanism, which is actually the macroscopic manifestation of the initiation, propagation, polymerization, and interaction of internal microcracks and microdefects under loading (Eberhardt 1998). The deformation characteristics of rock are closely related to the stress state and loading history (Singh and Digby 1989). Figure 12 shows the crack patterns on the surfaces of three kinds of multi-stage loading specimens, of which the  $50 \times 50$  mm<sup>2</sup> surface is the  $\sigma_1$  loading surface and the  $50 \times 100$  mm<sup>2</sup> surface is the  $\sigma_2$  loading surface. Notably, macrocracks are mainly produced during the last stage of loading. The stress conditions in the last stages of the three kinds of multi-stage loading discussed here are as follows: (a)  $\sigma_3 = \sigma_2 = 30$  MPa; (b)  $\sigma_3 = 30$  MPa and  $\sigma_2 = 65$  MPa; and (c)  $\sigma_3 = \sigma_2 = 0$  MPa.

The cracks on the  $\sigma_2$  loading surface of the multi-stage loading tests with increasing  $\sigma_2$  and increasing  $\sigma_3$  are basically the same, mainly Y-shaped cracks (tensile–shear mixed

failure). There are three relatively regular main fracture surfaces on the  $\sigma_2$  loading surface of these two samples, and these fractures converge at the end of the rock specimen. Due to the early postpeak unloading of the sample, as shown in Fig. 12a, except for the main fracture surface, the rock sample basically has no secondary crack surface, and the main crack on the left side has not completely penetrated the specimen. The crack development in the rock specimen shown in Fig. 12b is relatively sufficient, and a secondary crack surface is developed.

The main differences in the failure modes of the three multi-stage loading test specimens can be determined from the  $\sigma_1$  loading surface. In Fig. 12a, the crack morphology on the  $\sigma_1$  loading surface of the specimen is also Y-shaped. Multiple cracks develop at an angle between the  $\sigma_1$  and  $\sigma_2$  directions, and no penetration occurs. Only the cracks in the direction nearly parallel to the  $\sigma_2$  direction develop to one end of the loading surface. In Fig. 12b, several cracks nearly parallel to  $\sigma_2$  are developed on the  $\sigma_1$  loading surface, and the main crack crosses

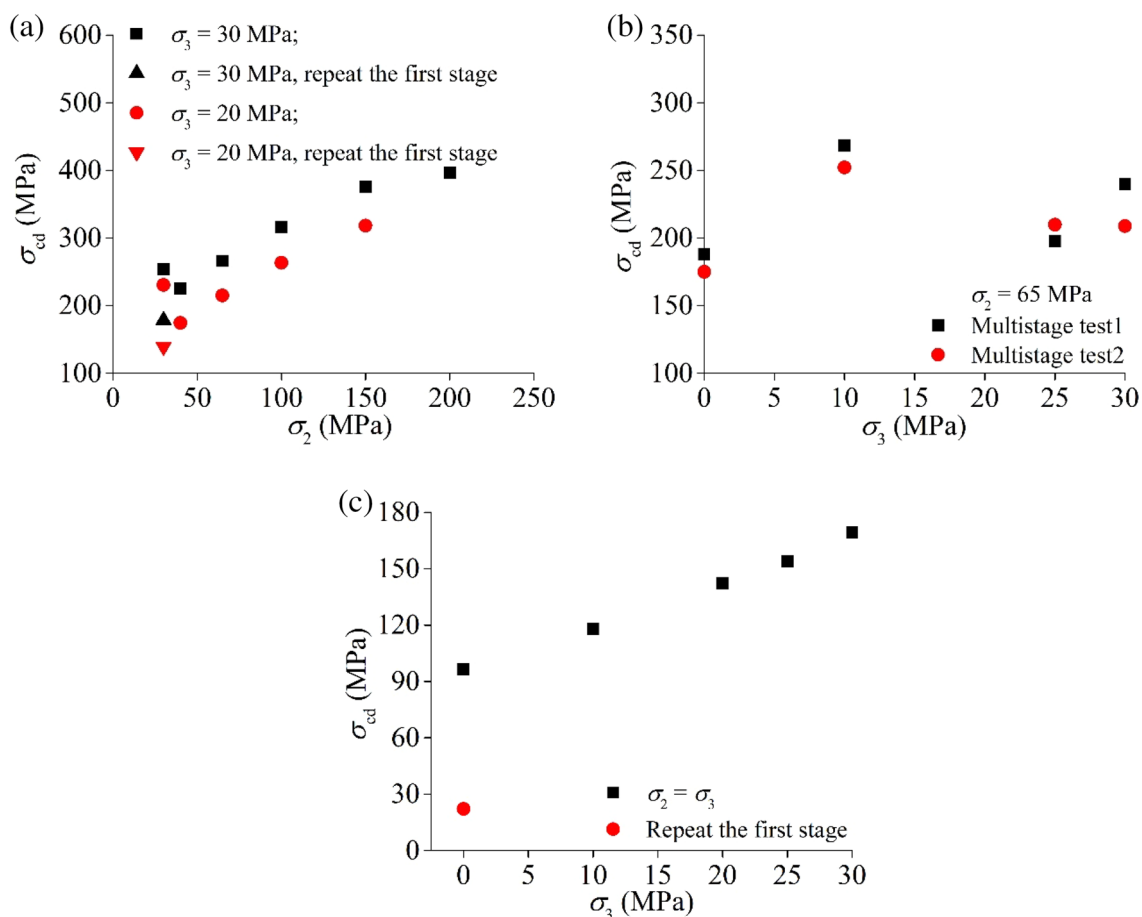


**Fig. 9**  $\sigma_{cd}$  of Jinping marble from the true triaxial multi-stage loading tests. **a** Increasing  $\sigma_2$ . **b** Increasing  $\sigma_3$ . **c** Increasing  $\sigma_2$  and  $\sigma_3$

the whole loading surface. The crack development of the conventional triaxial multi-stage loading specimen on the  $\sigma_1$  loading surface is more complex. The main cracks run across the whole  $\sigma_1$  loading surface in the directions of  $\sigma_3$  and  $\sigma_2$ , and the main cracks coalesce.

The results show that although the last stage of the multi-stage loading test with increasing  $\sigma_2$  is a conventional triaxial compression test, its failure mode is affected by the microfracturing caused by the previous stages of loading, reflecting the failure mode of a true triaxial stress compression test; however, the influence is limited, and the crack that developed along an angle between  $\sigma_1$  and  $\sigma_2$  can also be observed on the  $\sigma_1$  loading surface. For the multi-stage loading test with increasing  $\sigma_3$ , the specimen is always in the true triaxial stress state, so it corresponds to the typical true triaxial compression failure mode. The last stage of the conventional triaxial multi-stage loading test is uniaxial loading, but crack development is more complex in this stage due to the influence of the shear microcrack.

## 5 Discussion

In this study, the unloading point strength and peak strength in the last stage of conventional triaxial multi-stage loading are lower than those in the first stage, but the unloading point strength and peak strength in the last stage of true triaxial multi-stage loading with increasing  $\sigma_2$  are higher than those in the first stage (Fig. 13). The reasons for this pattern may be as follows.

1. The influence of  $\sigma_3$ . In the process of increasing  $\sigma_2$  during true triaxial multi-stage loading, microfracturing will occur in the direction perpendicular to  $\sigma_3$ , but since  $\sigma_3$  remains unchanged, the microfracture surface consistently bears an equivalent normal force. After unloading  $\sigma_1$  and  $\sigma_2$ , the microfracture will no longer continue to develop, but the influence of  $\sigma_3$  will further compact the microfracture, restrain the slip between the two surfaces, and increase the peak strength of the specimen. The last

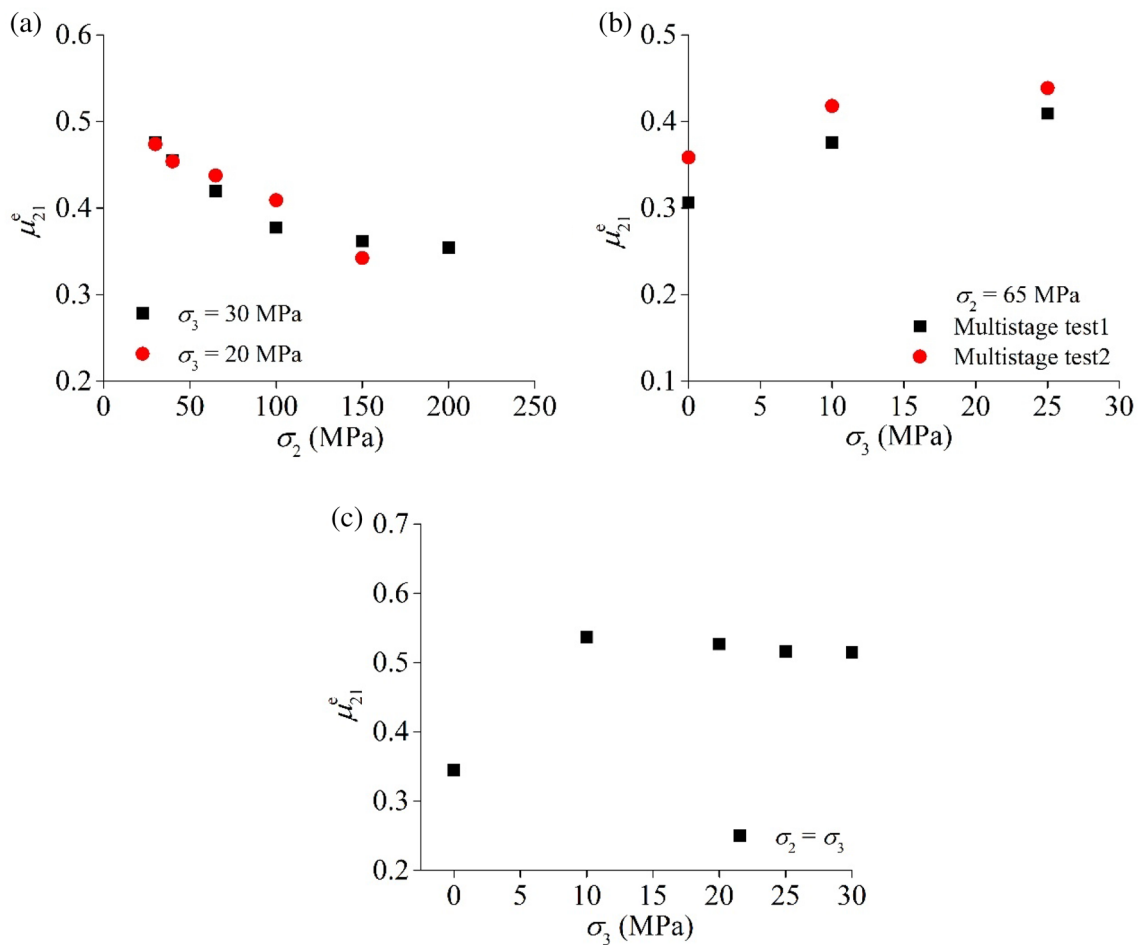


**Fig. 10** Poisson's ratio in the direction of the intermediate principal stress. **a** Increasing  $\sigma_2$ . **b** Increasing  $\sigma_3$ . **c** Increasing  $\sigma_2$  and  $\sigma_3$

stage of the multi-stage conventional triaxial test is equivalent to a complete uniaxial compression test, and the normal force of the microfracture surface is almost zero. During the confining pressure unloading process, due to the unloading effect, the microfracture may also undergo tip expansion, so the “weakening” phenomenon of Jinping marble occurred in the later stage.

2. The effect of axial unloading. Due to unloading before the peak strength, only microcracks are produced in the specimen. During loading, the local stress concentration between grains will produce debris. During axial unloading, the debris may fall off and fill the microcracks. When loaded again, the microfractures readjust, and the debris improves the contact state of the microfracture surface, restrains the slip between the microfracture surfaces, and increases the frictional strength between the microfracture surfaces. Uniaxial compression results in splitting failure, while the conventional triaxial compression results in shear failure. Axial unloading mainly increases the bearing capacity of the shear friction of microfracture surfaces in rock.

Therefore, axial unloading has a limited effect on the increase in uniaxial compressive strength and increases the strength under the conventional triaxial compression. That is, the uniaxial compressive strength is mainly weakened by microfractures, resulting in strength reduction in the last stage, while the conventional triaxial shear strength is both weakened and strengthened, and the last stage may produce a slight increase in strength.

## 6 Conclusions

An extensive investigation was carried out to study the validity of rapid procedures used to obtain the mechanical parameters of Jinping marble using true triaxial multi-stage loading tests. Based on the results of three kinds of multi-stage loading tests performed on Jinping marble, this paper studied the multi-stage loading strength, deformation characteristics, and failure mode of the marble. The following conclusions are made based on the test results.

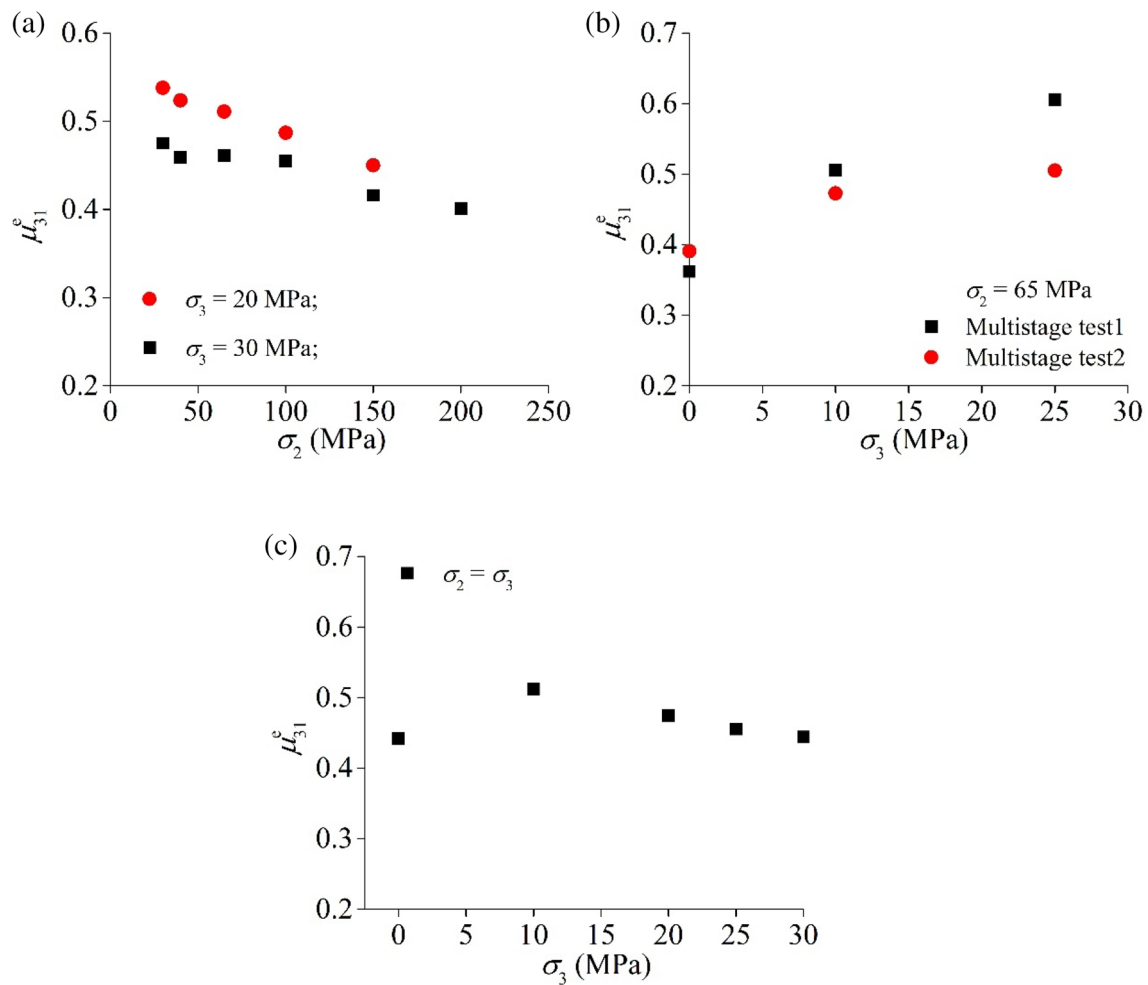


**Fig. 11** Poisson's ratio in the direction of the minimum principal stress. **a** Increasing  $\sigma_2$ . **b** Increasing  $\sigma_3$ . **c** Increasing  $\sigma_2$  and  $\sigma_3$

The reliability of the Jinping marble true triaxial multi-stage loading test is validated. Due to unloading under a fixed condition before the peak strength, the strength obtained from the multi-stage loading test is slightly lower than that obtained from the single-stage loading test, but the difference between the two strength parameters obtained by the Mogi–Coulomb criterion fitting is very small. In engineering practice, these differences are usually negligible.

The true triaxial multi-stage loading test is suitable for marble with obvious plastic sections, but the applicability of other types of hard rock needs to be further studied. During the test, the unloading point should not exceed the peak strength of the specimen to reduce the influence of microfracturing on the strength results. In the results of

the last stage of the multi-stage loading test, the potential error of the strength parameters can be evaluated to verify the reliability of the data selected by the slope. The Jinping marble multi-stage loading test exhibits good repeatability and can obtain reliable strength parameters in a short time for reference in engineering practice.

The test results show that the macromechanical properties of Jinping marble under different multi-stage loading conditions are closely related to the development of internal microcracks. Through the analysis of the failure mode, we know that the macrofailure mode of the specimen under true triaxial multi-stage loading is affected by internal microcrack growth. The influence of the internal micromechanical properties on the macromechanical performance of the rock needs to be further studied.

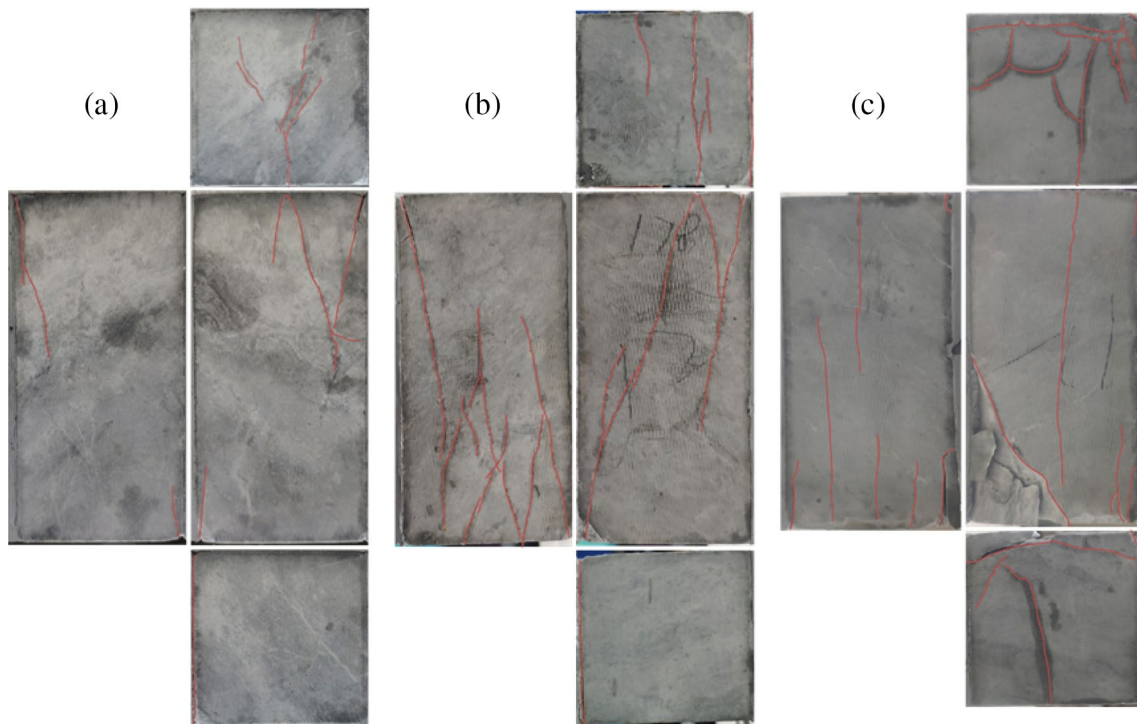


Fig. 12 Typical failure photos. **a** Increasing  $\sigma_2$ . **b** Increasing  $\sigma_3$ . **c** Increasing  $\sigma_2$  and  $\sigma_3$

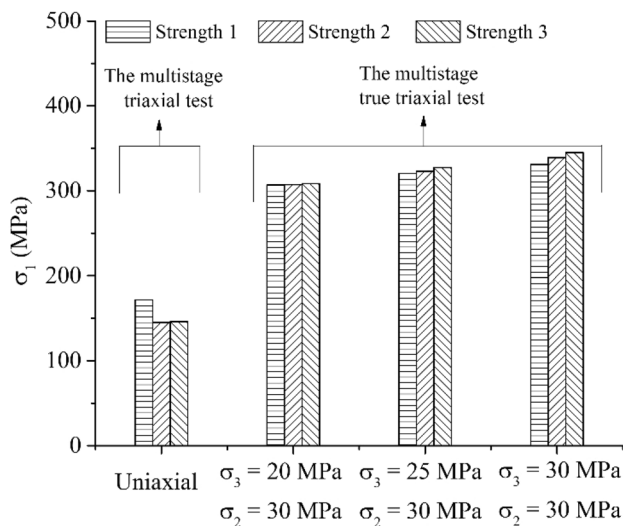


Fig. 13 Strength difference comparison (strength 1, unloading point strength of the first stage; strength 2, unloading point strength of the last stage; strength 3, peak strength of the last stage)

**Acknowledgements** The authors sincerely acknowledge financial support from the National Natural Science Foundation of China under Grant no. 51839003, Liao Ning Revitalization Talents Program under Grant No. XLYC1801002, and 111 Project under Grant no. B17009.

The authors are very grateful to Mr. Xiwei Zhang, Mr. Hong Xu, Mr. Yan Zhang, and Mr. Xufeng Liu for their great assistance.

**Declarations**

**Conflicts of Interest** The authors declare that they have no conflicts of interest.

**References**

Al-Ajmi AM, Zimmerman RW (2005) Relation between the mogi and the coulomb failure criteria. *Int J Rock Mech Min Sci* 42:431–439

Al-Ajmi AM, Zimmerman RW (2006) Stability analysis of vertical boreholes using the Mogi-Coulomb failure criterion. *Int J Rock Mech Min Sci* 43:1200–1211

Bondarenko TM, Hou B, Chen M, Yan L (2017) Laboratory research of fracture geometry in multi-stage HFF in triaxial state. *Mech Solids* 52:289–298

Chang C, Haimson B (2000) True triaxial strength and deformability of the german continental deep drilling program (ktb) deep hole amphibolite. *J Geophys Res Solid Earth* 105:18999–19013

Dassanayake ABN, Fujii Y, Fukuda D, Kodama JI (2015) A new approach to evaluate effective stress coefficient for strength in kimachi sandstone. *J Petrol Sci Eng* 131:70–79

Eberhardt E (1998) Brittle rock fracture and progressive damage in uniaxial compression. Dissertation, University of Saskatchewan

Feng XT (2017) Rockburst: mechanisms, monitoring, warning, and mitigation. Butterworth-Heinemann, Oxford

- Feng XT, Zhang X, Kong R, Wang G (2016) A novel mogi type true triaxial testing apparatus and its use to obtain complete stress-strain curves of hard rocks. *Rock Mech Rock Eng* 49:1649–1662
- Feng XT, Haimson B, Li XC, Chang CD, Ma XD, Zhang X, Ingraham M, Suzuki K (2019a) ISRM suggested method: determining deformation and failure characteristics of rocks subjected to true triaxial compression. *Rock Mech Rock Eng* 52:2011–2020
- Feng XT, Kong R, Yang C, Zhang X, Wang Z, Han Q, Wang G (2019b) A three-dimensional failure criterion for hard rocks under true triaxial compression. *Rock Mech Rock Eng* 53:103–111
- Feng XT, Gao Y, Zhang X, Wang Z, Zhang Y, Han Q (2020) Evolution of the mechanical and strength parameters of hard rocks in the true triaxial cyclic loading and unloading tests. *Int J Rock Mech Min Sci* 131(6):104349
- Feng XT, Wang Z, Zhou Y, Yang C, Pan P, Kong R (2021) Modelling three-dimensional stress-dependent failure of hard rocks. *Acta Geotech* 16:1–31
- Kim MM, Ko HY (1979) Multistage triaxial testing of rocks. *Geotech Test J* 2:98–105
- Kong R, Feng XT, Zhang X, Yang C (2018) Study on crack initiation and damage stress in sandstone under true triaxial compression. *Int J Rock Mech Min Sci* 106:117–123
- Kovari K, Tisa A, Einstein HH, Franklin JA (1983) Suggested methods for determining the strength of rock material in triaxial compression: revised version. *Int J Rock Mech Min Sci Geomech Abstr* 20:285–290
- Li Z, Sheng Y, Reddish DJ (2005) Rock strength reduction and its potential environmental consequences as a result of groundwater rebound. In: *The 9th International mine water congress*. Oviedo, Asturias, Spain, pp 513–519
- Martin CD (1997) Seventeenth Canadian geotechnical colloquium: the effect of cohesion loss and stress path on brittle rock strength. *Can Geotech J* 34:698–725
- Mogi K (1977) Dilatancy of rocks under general triaxial stress state with special reference to earthquake precursors. *J Phys Earth* 25:S203–S217
- Pagoulatos A (2004) Evaluation of multi-stage triaxial testing on Berea Sandstone. Dissertation, University of Oklahoma
- Singh UK, Digby I PJ (1989) A continuum damage model for simulation of the progressive failure of brittle rocks. *Int J Solids Struct* 25:647–663
- Taylor DW (1951) A triaxial shear investigation on a partially saturated soil. *ASTM Spec Tech Publ* 106:180–187
- Tsoi PA, Homenok IP (2017) Study of deformation-strength properties of sandstone under multi-stage triaxial compression. IOP Publishing PhysicsWeb, Bristol
- Wild KM, Barla M, Turinetti G, Amann F (2017) A multi-stage triaxial testing procedure for low permeable geomaterials applied to Opalinus clay. *J Rock Mech Geotech Eng* 9:519–530
- Xu H, Feng XT, Yang C, Zhang X, Zhou Y, Wang Z (2019) Influence of initial stresses and unloading rates on the deformation and failure mechanism of Jinping marble under true triaxial compression. *Int J Rock Mech Min Sci* 117:90–104
- Yang SQ (2012) Strength and deformation behavior of red sandstone under multi-stage triaxial compression. *Can Geotech J* 49:694–709
- Youn H, Tonon F (2010) Multi-stage triaxial test on brittle rock. *Int J Rock Mech Min Sci* 4:678–684
- Zhang Y, Feng XT, Zhang X, Wang Z, Sharifzadeh M, Yang C (2019a) A novel application of strain energy for fracturing process analysis of hard rock under true triaxial compression. *Rock Mech Rock Eng* 52:1–16
- Zhang Y, Feng XT, Yang C, Zhang X, Sharifzadeh M, Wang Z (2019b) Fracturing evolution analysis of Beishan granite under true triaxial compression based on acoustic emission and strain energy. *Int J Rock Mech Min Sci* 117:150–161

**Publisher's Note** Springer Nature remains neutral with regard to jurisdictional claims in published maps and institutional affiliations.